



HAL
open science

Magnetic anisotropies in oblique columnar growth of FeCoB films

Abdel Majid Aldimassi, Alexis Chevalier, Jamal Ben Youssef, Vincent Laur, Bruno Rouvellou

► **To cite this version:**

Abdel Majid Aldimassi, Alexis Chevalier, Jamal Ben Youssef, Vincent Laur, Bruno Rouvellou. Magnetic anisotropies in oblique columnar growth of FeCoB films. *AIP Advances*, 2020, 10 (6), pp.065218. 10.1063/5.0003895 . hal-03206381

HAL Id: hal-03206381

<https://hal.science/hal-03206381>

Submitted on 23 Apr 2021






HAL is a multi-disciplinary open access archive for the deposit and dissemination of scientific research documents, whether they are published or not. The documents may come from teaching and research institutions in France or abroad, or from public or private research centers.

L'archive ouverte pluridisciplinaire **HAL**, est destinée au dépôt et à la diffusion de documents scientifiques de niveau recherche, publiés ou non, émanant des établissements d'enseignement et de recherche français ou étrangers, des laboratoires publics ou privés.

Magnetic anisotropies in oblique columnar growth of FeCoB films

Cite as: AIP Advances **10**, 065218 (2020); <https://doi.org/10.1063/5.0003895>

Submitted: 05 February 2020 . Accepted: 21 May 2020 . Published Online: 11 June 2020

A. M. Aldimassi , A. Chevalier , J. Ben Youssef , V. Laur , and B. Rouvellou 

COLLECTIONS

Paper published as part of the special topic on [Chemical Physics](#), [Energy, Fluids and Plasmas](#), [Materials Science](#) and [Mathematical Physics](#)



View Online



Export Citation



CrossMark

ARTICLES YOU MAY BE INTERESTED IN

[Enhanced soft magnetic properties in CoZrTa\(B\) thin film with improving amorphous structure via introducing B atoms](#)

AIP Advances **10**, 065109 (2020); <https://doi.org/10.1063/5.0006063>

[Magneto-optical Kerr microscopy investigation of magnetization reversal in Co₂FeSi Heusler alloy thin films](#)

AIP Advances **10**, 065017 (2020); <https://doi.org/10.1063/5.0002408>

[Surface-sensitive magnetic characterization technique for ultrathin ferromagnetic film with perpendicular magnetic anisotropy](#)

AIP Advances **10**, 065019 (2020); <https://doi.org/10.1063/5.0012321>

AIP Advances Nanoscience Collection

READ NOW!

Magnetic anisotropies in oblique columnar growth of FeCoB films

Cite as: AIP Advances 10, 065218 (2020); doi: 10.1063/5.0003895

Submitted: 5 February 2020 • Accepted: 21 May 2020 •

Published Online: 11 June 2020



View Online



Export Citation



CrossMark

A. M. Aldimassi,  A. Chevalier,  J. Ben Youssef,  V. Laur,  and B. Rouvellou^{a)} 

AFFILIATIONS

Lab-STICC, UMR CNRS 6285, Université de Bretagne Occidentale, 6 Avenue Le Gorgeu, CS93837, 29238 Brest Cedex 3, France

^{a)} Author to whom correspondence should be addressed: bruno.rouvellou@univ-brest.fr

ABSTRACT

We report on the evolution of anisotropies of FeCoB thin films deposited by magnetron sputtering with different oblique angles increasing from $\alpha = 0^\circ$ to $\alpha = 75^\circ$. The oblique incidence deposition using the $\text{Fe}_{43}\text{Co}_{43}\text{B}_{14}$ target leads, under chosen conditions, to columnar growth without bundling. This columnar structure results in a correlated increase in the anisotropy field and of the resonance frequency values, observed with an increasing oblique incidence angle from $\alpha = 0^\circ$ to $\alpha = 45^\circ$. However, these values decrease from $\alpha = 45^\circ$ to $\alpha = 75^\circ$. To get a better understanding of the reversal magnetization process, in plane angular distribution of different magnetic parameters was carried out, and the role of easy axis dispersion was especially investigated. The optimized conditions of deposition, leading to controlled high resonance frequencies, could be useful in the design of FeCoB-based microwave devices.

© 2020 Author(s). All article content, except where otherwise noted, is licensed under a Creative Commons Attribution (CC BY) license (<http://creativecommons.org/licenses/by/4.0/>). <https://doi.org/10.1063/5.0003895>

I. INTRODUCTION

Soft magnetic thin films are widely used as passive chip components in microwave circuits in the field of telecommunications or non-contact sensors. High levels of miniaturization, efficiency, and integration are required for these passive components. The miniaturization factor of microwave devices is linked to the guided wavelength and thus to the permeability of the material. As a consequence, these soft magnetic films must present high permeability together with high resonance frequency. FeCoB magnetic thin films are good candidates for gigahertz application,¹ allowing achievement of high saturation magnetization, $4\pi M_s$.² This characteristic is crucial for the miniaturization of high frequency devices because it leads to high permeability values. According to the Kittel equation,³ the resonance frequency can be tuned by the magnetic anisotropy field, H_k . Recent works have focused on obtaining a high value of uniaxial anisotropy field. In order to obtain a high anisotropy field, there are several methods such as magnetic field annealing,⁴ exchange bias coupling,⁵ pre-stressed materials,⁶ and oblique deposition.⁷ One of the easiest ways to tune the uniaxial anisotropy field is the oblique deposition by magnetron sputtering.⁸

A thin film elaborated by a vapor beam with oblique-angle incidence forms a columnar structure, which is very different from

a continuous film grown under normal incidence. Because of the shadowing effect and limited surface diffusion, oblique deposition of a magnetic film results in the formation of columns which tend to coalesce in the direction perpendicular to the deposition plane. The columnar grain structure induces magnetic anisotropy through the shape anisotropy of columnar grains. The observed character of H_k is related to the two processes occurring during film growth: the field is parallel to the column axis or perpendicular to the incidence plane, and it indicates the degrees of the columnar growth and the bundle formation of columnar grains. In addition, the crystalline texture of the samples has to be taken into account.⁹ However, a better understanding of the magnetic properties of such films needs information about easy axis dispersion.¹⁰

Recently, Li *et al.*¹¹ demonstrated the relevance of using the FeCoB alloy to obtain tunable magnetic properties by oblique deposition. In their study, the FeCoB boron concentration is equal to 3.2%, and the easy axis lies perpendicular to the incidence plane. In the present work, to eliminate crystal anisotropy from parameters, the boron concentration is increased up to 14%, which leads to obtaining amorphous material.¹² Furthermore, boron is known to segregate at grain boundaries.¹³ A higher boron concentration may hence allow the growth of independent columns without bundling.

In this paper, we characterize the structure and morphology of thin films obtained by magnetron sputtering of the $\text{Fe}_{43}\text{Co}_{43}\text{B}_{14}$ target. The evolution of static and dynamic magnetic properties of the nanostructured thin film with the incidence deposition angle is analyzed. More specifically, the role of easy axis dispersion is investigated and discussed.

II. EXPERIMENTAL DETAILS

Samples were grown on a $9 \times 9 \text{ mm}^2$ Si (100) substrate with radio frequency (RF) magnetron sputtering using the $\text{Fe}_{43}\text{Co}_{43}\text{B}_{14}$ target. The RF power was 50 W for a 3 in. diameter target, the argon flow was maintained at 8 SCCM corresponding to a pressure of 9×10^{-3} mbar, and the residual pressure in the sputtering chamber was about 3×10^{-7} mbar. These conditions resulted from an optimization made on the coercive field. The deposits were realized under a very weak magnetic field (around 5 G at the substrate position) mainly generated by the magnetron. The samples studied here were obtained with four angles of incidence α of the vapor flux relative to the substrate normal direction, varying from 0° to 75° . For oblique incidence, the substrates were placed on beveled holders having different inclination angles from 25° to 75° . In order to preserve the deposition direction, all samples were marked at their rear sides. Each FeCoB sample was deposited for around 1 h, adjusting the time to obtain a thickness of about 150 nm. A 4 nm SiO_2 layer was added to protect the material from oxidation and to avoid degradation of the magnetic properties. Thus, due to native SiO_2 , FeCoB samples include two symmetrical interfaces: Si/ SiO_2 /FeCoB and FeCoB/ SiO_2 . Deposition rates were verified by a thickness profilometer.

The structure of the materials was analyzed using x-ray diffraction (XRD PANalytical-empyrean diffractometer with Cu-K α radiation). The surface morphology was imaged using noncontact atomic force microscopy (AFM Nanoscope V multimode, Digital Instruments, Veeco) operated in the peak force tapping mode. A vibrating sample magnetometer (VSM) was used to measure the magnetization of the sample simultaneously parallel and perpendicular to the applied field, i.e., the longitudinal magnetization M_l and transversal magnetization M_t . The value of H_k was extracted from the recorded hysteresis loops (i) by calculating the measured area of easy axis and hard axis loops of reduced magnetization¹⁴ and (ii) from the slope of the rotational-like magnetization curve on the hard axis loop. These two methods lead to very close values that have been averaged. The angular dependence of the remanent magnetization M_r achieved by angular remanence measurements (ARM) was used to obtain the angular dispersion of the anisotropy.¹⁵ The ARM were performed by varying the field angle φ from 0° to 180° , with 0° being the easy axis direction. For each φ , a strong field was applied to saturate the sample and then was switched off. The remanence along the easy direction was measured by rotating the sample to 0° . Dynamic permeability was measured using a shorted microstrip permeameter¹⁶ and a network analyzer. To take into account the influence of substrate permittivity and the magnetic film and the effects of film conductivity, a reference measurement is added to the experimental procedure. The sample is measured by saturating the permeability along the microwave field direction by a strong external static field to obtain the reference measurement.

III. RESULTS AND DISCUSSION

Figure 1 shows the x-ray diffraction measurement obtained for the four samples. All XRD spectra show a very weak and large peak corresponding to the FeCoB line (110) around an angle 2θ between 43° and 45° . This peak belongs to the bcc CoFe phase. The lattice spacing remains almost the same and does not vary with various oblique angles.

Observation of the x-ray diffraction pattern is an indication that FeCoB is amorphous or there are FeCoB nanocrystals embedded in the amorphous matrix. By measuring the full width at half maximum and using the Scherrer equation,¹⁷ the estimated grain size value is between 2 nm and 5 nm, as expected for such high boron content.

Figure 2 represents typical three dimensional images taken for the four samples, with the scanning area of AFM images being $0.5 \times 0.5 \mu\text{m}^2$.

Images show that the surface is made up of small grains grouped together to form clusters. The root mean square roughness R_q increases with the oblique angle, in a very low range from 0.225 nm ($\alpha = 0^\circ$) to 0.742 nm ($\alpha = 75^\circ$). The film at normal incidence appears like a smooth and continuous surface, whereas the surface is rougher and coarsens at an oblique angle. These latter broad mound-like surface features are characteristic of columnar growth.¹⁸ One should note the absence of any bundling features. Moreover, well separated columns generate a shape anisotropy field parallel to the column axis, and as a result, the in plane easy axis should lie in the incident direction. It was indeed observed in all M–H loops recorded for oblique incidence samples.

$4\pi M_s$, obtained by the total saturated magnetic moments and the volume of the thin films, is, for all samples, about 16 kG. Figure 3 shows the hysteresis loops of the FeCoB films elaborated with different oblique angles α , where the magnetization is normalized to M_s .

In-plane measurements are mainly characteristics of in-plane uniaxial magnetic anisotropy. However, if the M–H loops along

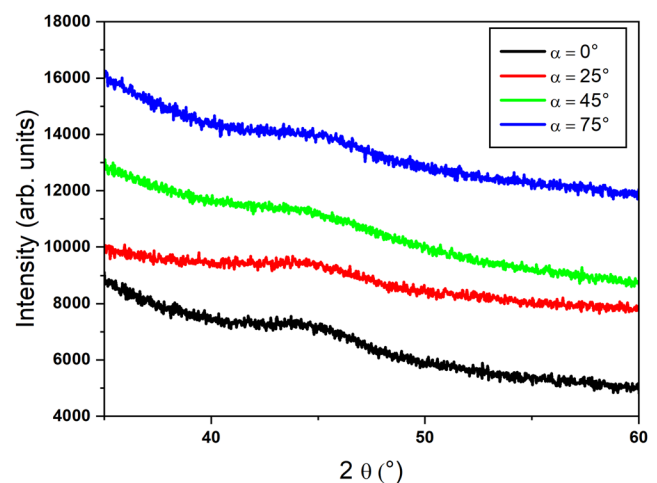


FIG. 1. X-ray diffraction patterns of FeCoB deposited with different incident angles α .

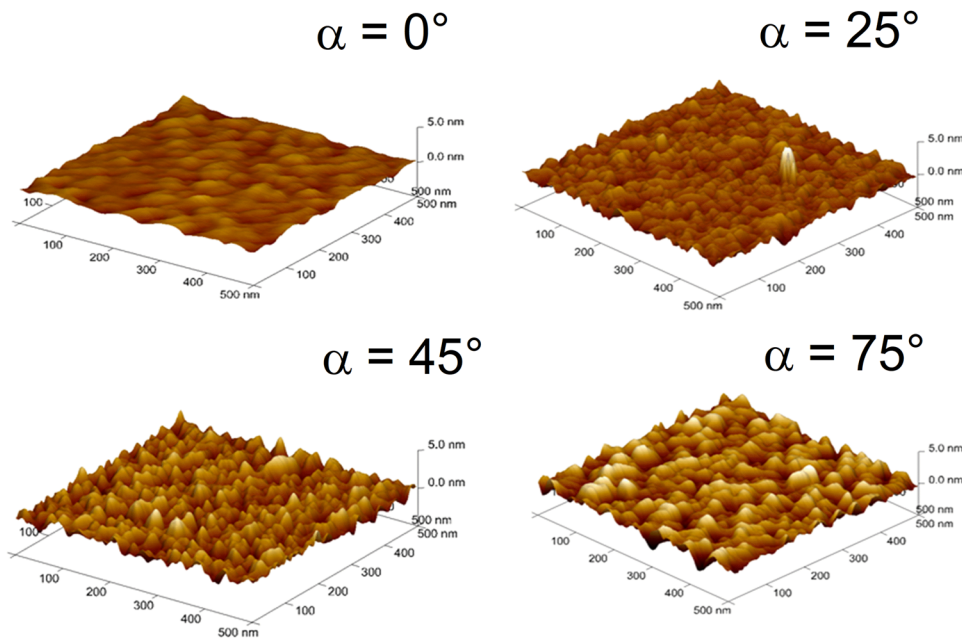


FIG. 2. 3D AFM images of FeCoB deposited with different incident angles.

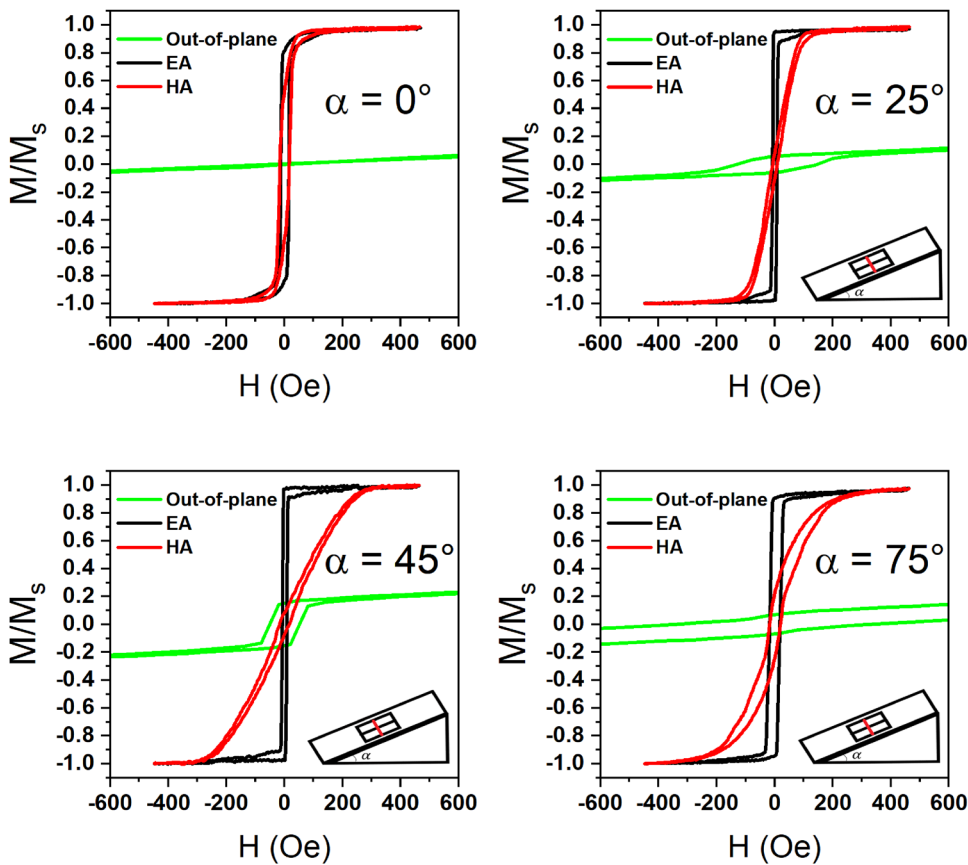


FIG. 3. Hysteresis loops of FeCoB deposited with different incident angles: out-of-plane (green line), in plane along the easy axis (black line), and that along the hard axis (red line).

the easy axis have a rectangular shape, the slight opening of the hard axis hysteresis loops may reflect an angular dispersion of the anisotropy.¹⁵ Moreover, the coercivity H_c depends on the root mean square roughness and on the nanocrystal grain size.¹⁹ For oblique incidence growth, the increase in the roughness R_q with an increasing deposit angle measured by AFM is correlated with a similar increase in the coercivity H_c , observed in Fig. 3, especially along the hard axis.

All out-of-plane loops show saturation at about 17 kOe. In the zero field regions, shown in Fig. 3, one can observe an opening of the out-of-plane loops. This opening is the signature of an out-of-plane component of the anisotropy. This component may be due to the columnar shape, and indeed, the opening is not present at normal incidence ($\alpha = 0^\circ$) and is larger at $\alpha = 25^\circ$ than at $\alpha = 45^\circ$. However, it is increasing at $\alpha = 75^\circ$. Moreover, for this incidence angle, the M-H loops display a pronounced change in the slope along the in plane hard axis that can reveal either perpendicular anisotropy²⁰ or/and angular dispersion of the in plane anisotropy.¹⁵ Despite this change in the slope, the two methods used to extract the values of H_k from the hysteresis loops lead, even in this case, to very close values.

For different incidence angles, Fig. 4(a) displays the anisotropy field H_k values and the corresponding calculated resonance frequencies $f_{r,calc}$ together with measured frequencies $f_{r,exp}$ extracted from the microwave permeability spectra, presented in Fig. 4(b).

The in-plane anisotropy field values increase with the oblique deposition angle up to 45° . Such an increase, already observed in Refs. 11 and 21, can be explained by an increase in the in-plane component of the columnar shape anisotropy. For an incident angle of 75° , the lowering of the measured in-plane anisotropy can be attributed to interface stress due to the significant film thickness gradient measured across the sample. Indeed, the thickness gradient is two or three times higher in the $\alpha = 75^\circ$ sample than in other samples, where the thickness varies along the incident direction from +15% to -15% of the nominal value. Wu *et al.*²² showed that when FeCoB is grown on the Si surface with a thickness gradient, a compressive stress is produced at the interface along the thickness gradient direction. The observed reduced value of the anisotropy along the incidence direction may then result from the stress induced alignment of magnetic moments perpendicular to that direction.

The resonance frequency is calculated by

$$f_r = \frac{\gamma}{2\pi} \sqrt{4\pi M_s \cdot H_k}, \quad (1)$$

where $\gamma = 2.8$ GHz/kOe is the gyromagnetic ratio. One should note the uncertainties resulting from the weakness of the permeability signal measured for $\alpha = 75^\circ$. This weak signal can be explained by high damping. Indeed, if Lorentzian fitting is used to obtain the full width at half-maximum (FWHM) of μ'' , for $\alpha = 0^\circ$ and $\alpha = 75^\circ$, the FWHM is about 2 GHz, while for $\alpha = 25^\circ$ and $\alpha = 45^\circ$, the FWHM is less than 1 GHz. Because the saturation magnetization $4\pi M_s$ is almost constant and close to 16 kG, the evolution of the calculated frequencies follows the evolution of H_k with the incidence angle. The calculated and experimental frequencies are in good agreement from 0° to 45° . The difference between calculated (4.7 GHz) and experimental (about 3 GHz) frequencies at 75° can be explained by the experimental limitation; in this case, the sample should not be fully saturated by the static field of 1 kOe applied in the reference procedure. As mentioned above, perpendicular contribution of anisotropy may be significant for $\alpha = 75^\circ$, and the $M_r/M_s = 0.89$ value along the easy axis is different from unity unlike for other samples. To evaluate this contribution, we carried out additional ferromagnetic resonance (FMR) measurements in a 3–35 GHz broad band. The measured evolution of the FMR field in a planar geometry up to 6 kOe as a function of resonance frequency (not shown) allows extracting the effective magnetization,²³

$$4\pi M_{eff} = 4\pi M_s - \frac{2K_{\perp}}{M_s}. \quad (2)$$

The perpendicular contribution is negligible for all samples except for $\alpha = 75^\circ$, for which $\frac{2K_{\perp}}{M_s}$ reaches a value close to 800 G.

To get a better understanding of the reversal magnetization process, in plane angular distribution of different magnetic parameters was carried out. Figure 5 shows the experimental azimuthal evolution of the normalized remanence M_r/M_s and normalized maximum transverse magnetization $M_{t,max}/M_s$. The azimuthal angle value $\varphi = 0^\circ$ corresponds to the easy axis direction.

The two lobe shapes of M_r/M_s , with maxima closed to 1 when the applied field is along the easy axis, are characteristics of in-plane uniaxial magnetic anisotropy. For transversal components, the ratio $M_{t,max}/M_s$ is minimal along the two axes. Along the hard axis, the

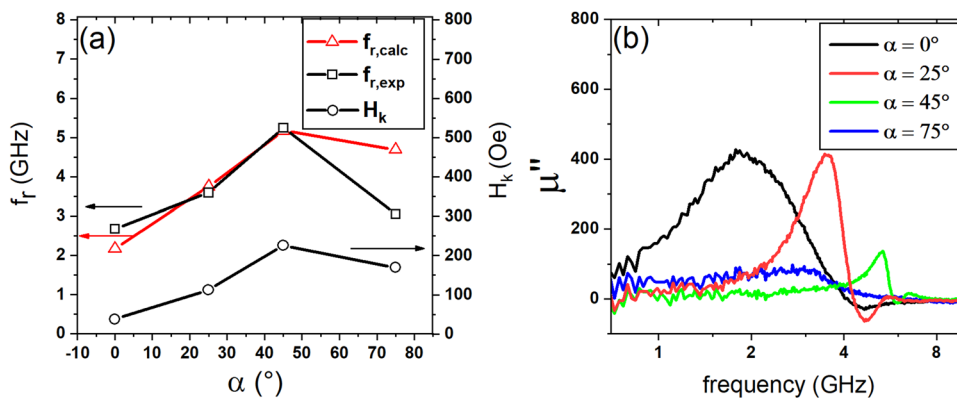


FIG. 4. FeCoB deposited with different incident angles α : (a) calculated (red triangle) and experimental (black square) resonance frequency and anisotropy (black bullet) and (b) imaginary permeability spectra measured along the hard axis.

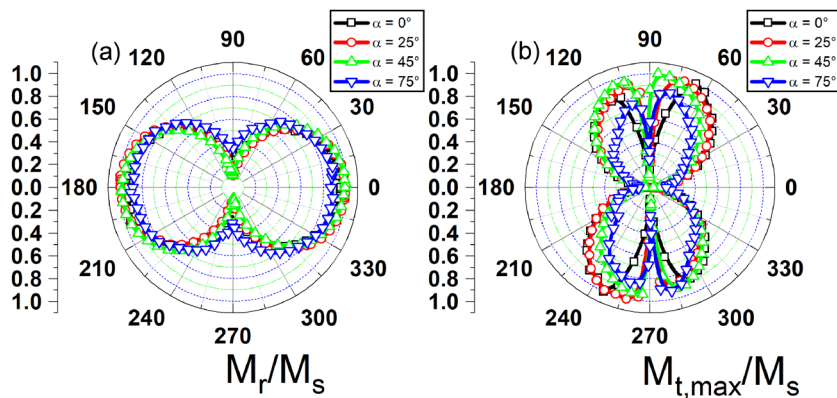


FIG. 5. Azimuthal evolution of the (a) remanence and (b) maximum transverse magnetization normalized to the magnetization saturation of FeCoB deposited with different incident angles α .

macrospin model is expected to correctly describe the magnetization reversal, with the macrospin rotating from saturation, M_s to $-M_s$, and being fully transversal at zero field. However, when the applied field is along the hard axis, M_r/M_s does not fall to zero, especially for $\alpha = 0^\circ$ and $\alpha = 75^\circ$, and $M_{t,max}/M_s$ is minima instead of maxima. As mentioned above, the possible angular dispersion of the anisotropy¹⁵ can explain the singularities observed along the hard axis. Moreover, these observations can be correlated with the high damping values observed for $\alpha = 0^\circ$ and $\alpha = 75^\circ$. Indeed, damping consists of intrinsic and extrinsic contributions, the latter being related to the inhomogeneities of magnetic anisotropy.²⁴ To gain further insight into these correlations, the values of angular dispersion are required.

Figure 6 shows the normalized angular dependence remanence $M_r/M_{r,max}$ obtained by ARM and its derivative, with φ being the angle between the applied field and the easy axis.

When the applied field is along the hard axis, $\varphi = 90^\circ$, and after removal of the field, the remanence along the easy axis should be zero due to the formation of equally distributed opposite magnetic grain orientation. A well-defined uniaxial anisotropy is characterized by a very sharp variation in $M_r/M_{r,max}$ near $\varphi = 90^\circ$ from 1 to -1 . The angular dependence of the derivative of $M_r/M_{r,max}$ with respect to φ is presented in Fig. 6(b). The angular dispersion issue from the derivative of the remanence defines a switching peak. If $\Delta\varphi_{10}$ defines a deviation of 10% from the maximum value of the

peak, $\Delta\varphi_{10}$ decreases from 26° for normal incidence ($\alpha = 0^\circ$) to less than 8° for oblique incidence angles. On the contrary to normal incidence, for $\alpha = 75^\circ$, the weak angular dispersion, $\Delta\varphi_{10} = 4^\circ$, is thus not an explanation of the measured high damping value. However, as shown in Fig. 6(a), a slight decreasing slope is observed only for $\alpha = 75^\circ$ from $\varphi = 0^\circ$ to $\varphi = 85^\circ$. In a similar case, Liu and Zangari¹⁵ concluded that the angular dependence of M_r is controlled by competition between the uniaxial anisotropy and the rotatable anisotropy due to the stripe domain structure. Thus, the slight slope could be explained by the fact that the stripe direction turns toward the easy axis gradually from $\varphi = 85^\circ$ to $\varphi = 0^\circ$. The possible formation of a weak stripe domain, when increasing the incidence angle from $\alpha = 45^\circ$ to $\alpha = 75^\circ$, may be induced by a corresponding increase in stress, as mentioned above. Moreover, the permeability spectra were recorded after saturation along the microwave field, i.e., in the hard axis remanent state. For oblique deposited films, according to Wang *et al.*,²⁵ the stripe direction at this remnant state is not aligned along the direction of the previously applied bias field but turns partially toward the easy axis direction. As a consequence, the stripe direction is not fully perpendicular to the microwave field, and one would explain the large resonance peaks observed in Fig. 4(b).

The much larger anisotropy dispersion measured for normal incidence ($\Delta\varphi_{10} = 26^\circ$) is related to the much larger dip, as observed

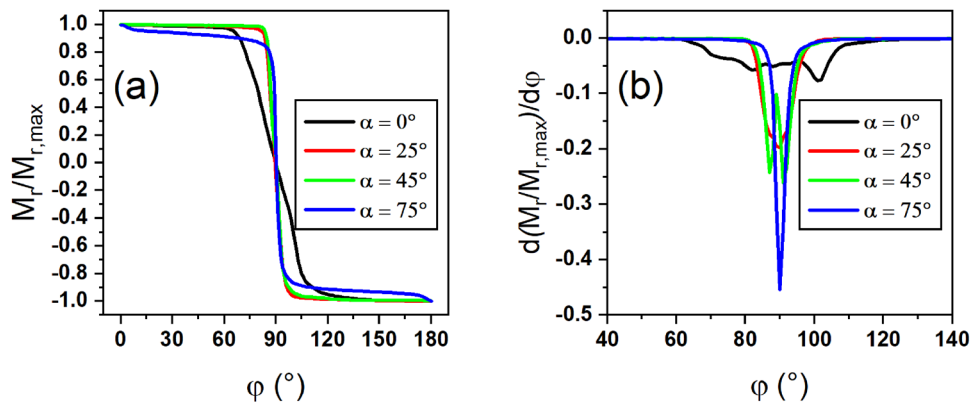


FIG. 6. (a) Angular dependence of normalized M_r remanence along the easy axis and (b) its derivative of FeCoB deposited with different incident angles α .

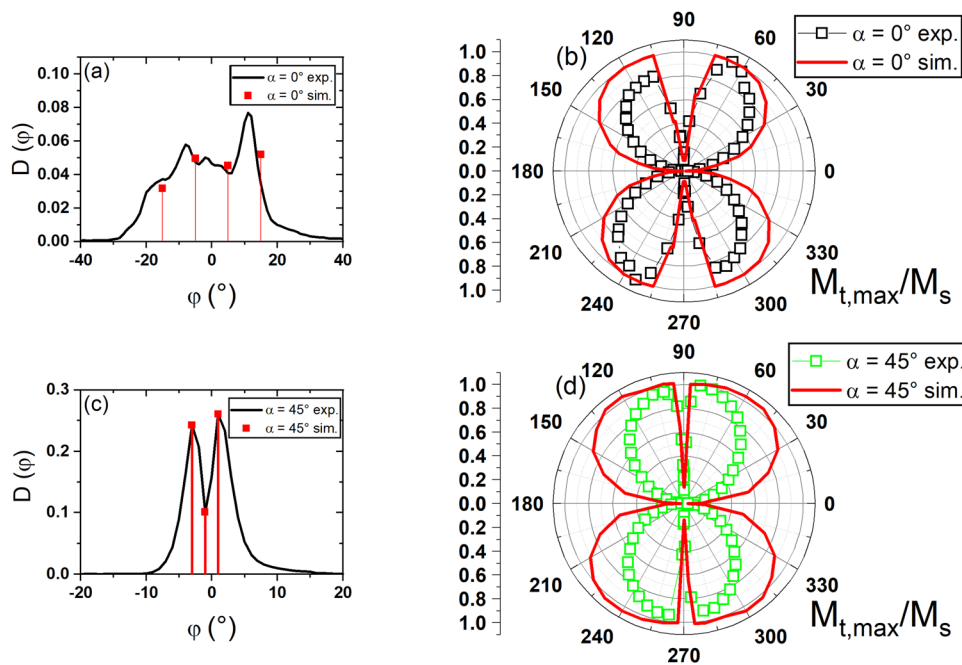


FIG. 7. Distributions of the anisotropy $D(\varphi)$ issue from ARM for (a) $\alpha = 0^\circ$ and (c) $\alpha = 45^\circ$ and corresponding experimental and theoretical azimuthal evolution of the maximum transverse magnetization normalized to saturation magnetization for (b) $\alpha = 0^\circ$ and (d) $\alpha = 45^\circ$.

in Fig. 5(b), around 90° in the angular distribution $M_{t,max}/M_s$. Such a correlation with angular distribution of $M_{t,max}/M_s$ can be explained by the results displayed Fig. 7, where a comparison is made between experimental angular distributions $M_{t,max}/M_s$ of $\alpha = 0^\circ$ and $\alpha = 45^\circ$ and the corresponding angular distributions calculated using the macrospin S&W equation^{26,27} and taking into account the measured angular dispersions.

A discretization of the angular distribution of anisotropy $D(\varphi)$, resulting from the ARM, is realized with 3 ($\alpha = 45^\circ$) or 4 ($\alpha = 0^\circ$) anisotropy fields, as shown in Figs. 7(a) and 7(c). Azimuthal evolutions $M_{t,max}/M_s$ are calculated for each macrospin independently governed by each corresponding anisotropy field. The weighted average of the angular distribution for these three or four macrospins has been calculated to determine the azimuthal evolution of $M_{t,max}/M_s$ (red line), shown in Figs. 7(b) and 7(d). The angular dispersion affects the azimuthal evolution of $M_{t,max}/M_s$ around 90° , and, consequently, the multiple macrospins model agrees well with the experimentally measured dips observed at 90° . This can be explained by the fact that each macrospin rotates clockwise or anti-clockwise depending on the sign with which the corresponding easy axis deviates from its nominal value. By moving away from these angles, the four macrospins and single macrospin models lead to similar azimuthal evolution.

IV. CONCLUSION

FeCoB thin films have been prepared by RF magnetron sputtering with a deposited oblique angle from $\alpha = 0^\circ$ to $\alpha = 75^\circ$. The AFM measurements and the direction of the easy axis indicate that the oblique incidence, under chosen conditions, leads to columnar growth without bundling. When increasing the angle of incidence

from $\alpha = 0^\circ$ to $\alpha = 45^\circ$, the increasing columnar shape anisotropy leads to an increase in H_k . As a consequence, the resonance frequency f_r increases, and a better defined anisotropy direction leads to a decrease in damping. When increasing the angle of incidence from $\alpha = 45^\circ$ to $\alpha = 75^\circ$, the magnetic properties are degraded due to the formation of a thickness gradient. This work highlights the possibility to control anisotropy field, and thus resonance frequency, of FeCoB thin films as a function of deposition conditions that can be used to fabricate dedicated soft magnetic films for microwave devices.

ACKNOWLEDGMENTS

The authors gratefully acknowledge the PIMM-DRX of Université de Bretagne Occidentale and its staff. This work was supported by the European Union through the European Regional Development Fund (ERDF), the Ministry of Higher Education and Research, the Région Bretagne, the Conseil général du Finistère, and Brest Métropole Océane, through CPER Project No. 2015-2020 MATECOM and by the Agence Nationale de la Recherche.

DATA AVAILABILITY

The data that support the findings of this study are available from the corresponding author upon reasonable request.

REFERENCES

- ¹K. Ikeda, K. Kobayashi, and M. Fujimoto, *J. Appl. Phys.* **92**, 5395 (2002).
- ²M. K. Minor, T. M. Crawford, T. J. Klemmer, Y. Peng, and D. E. Laughlin, *J. Appl. Phys.* **91**, 8453 (2002).
- ³C. Kittel, *Phys. Rev.* **71**, 270 (1947).

- ⁴K. Seemann, H. Leiste, and V. Bekker, *J. Magn. Magn. Mater.* **278**, 200 (2004).
- ⁵G. Chai, N. N. Phuoc, and C. K. Ong, *Sci. Rep.* **2**, 832 (2012).
- ⁶P. D. Thang, G. Rijnders, and D. H. A. Blank, *J. Magn. Magn. Mater.* **310**, 2621 (2007).
- ⁷X. Liu, Y. Zuo, X. Zhou, W. Li, L. Feng, and D. Yao, *J. Appl. Phys.* **117**, 103902 (2015).
- ⁸J. Li, Q. Zhan, S. Zhang, J. Wei, J. Wang, M. Pan, Y. Xie, H. Yang, Z. Zhou, S. Xie, B. Wang, and R.-W. Li, *Sci. Rep.* **7**, 2837 (2017).
- ⁹K. Okamoto, K. Itoh, and T. Hashimoto, *J. Magn. Magn. Mater.* **87**, 379 (1990).
- ¹⁰J. M. Alameda, M. Torres, and F. López, *J. Magn. Magn. Mater.* **62**, 209 (1986).
- ¹¹C. Li, G. Chai, C. Yang, W. Wang, and D. Xue, *Sci. Rep.* **5**, 17023 (2015).
- ¹²C. L. Platt, N. K. Minor, and T. J. Klemmer, *IEEE Trans. Magn.* **37**, 2302 (2001).
- ¹³E. Yu, J. S. Shim, I. Kim, J. Kim, S. H. Han, H. J. Kim, K. H. Kim, and M. Yamaguchi, *IEEE Trans. Magn.* **41**, 3259 (2005).
- ¹⁴A. Neudert, J. McCord, R. Schäfer, and L. Schultz, *J. Appl. Phys.* **95**, 6595 (2004).
- ¹⁵X. Liu and G. Zangari, *J. Appl. Phys.* **90**, 5247 (2001).
- ¹⁶D. Pain, M. Ledieu, O. Acher, A. L. Adenot, and F. Duverger, *J. Appl. Phys.* **85**, 5151 (1999).
- ¹⁷A. L. Patterson, *Phys. Rev.* **56**, 978 (1939).
- ¹⁸A. Amassian, K. Kaminska, M. Suzuki, L. Martinu, and K. Robbie, *Appl. Phys. Lett.* **91**, 173114 (2007).
- ¹⁹J. Zhu, K. Zhou, Y. Yang, D. Tang, B. Zhang, M. Lu, and H. Lu, *J. Magn. Magn. Mater.* **374**, 544 (2015).
- ²⁰M. Coisson, F. Celegato, E. Olivetti, P. Tiberto, F. Vinai, and M. Baricco, *J. Appl. Phys.* **104**, 033902 (2008).
- ²¹N. N. Phuoc, F. Xu, and C. K. Ong, *J. Appl. Phys.* **105**, 113926 (2009).
- ²²C. Wu, Y. Huang, Y. Cui, Z. Shen, Y. Ma, S. Xie, H. Du, X. Gao, and S. Li, *IEEE Trans. Magn.* **51**, 1 (2015).
- ²³J. Ben Youssef, J. Richey, N. Beaulieu, T. Hauguel, D. T. Dekadjevi, J.-P. Jay, D. Spenato, and S. P. Pogossian, *J. Phys. D: Appl. Phys.* **49**, 375001 (2016).
- ²⁴K. Seemann and H. Leiste, *J. Magn. Magn. Mater.* **321**, 742 (2009).
- ²⁵G. Wang, C. Dong, W. Wang, Z. Wang, G. Chai, C. Jiang, and D. Xue, *J. Appl. Phys.* **112**, 093907 (2012).
- ²⁶E. C. Stoner and E. P. Wolfarth, *Philos. Trans. R. Soc. London* **240**, 599 (1948).
- ²⁷M. Gloanec, S. Rioual, B. Lescop, R. Zuberek, R. Szymczak, P. Aleshkevych, and B. Rouvellou, *Phys. Rev. B* **82**, 144433 (2010).